Electronic Supplementary Information

Barium-induced lattice expansion of $Ni(OH)_2$: enhancing catalytic urea oxidation activity for energy-saving H_2 production

Cengceng Du[a], Zhenyu Wang[a], Yiming Wang[a], Wenjuan Xu[b,*], Yuqiu Huo[a,*], and Hongbin Sun[a,*], Guangwen Xu[c,d]

a, Department of Chemistry, Northeastern University, Shenyang 110819, People's Republic of China; E-mail: sunhb@mail.neu.edu.cn.
b, Central R&D Institute, LONGi Green Energy Technology Co.Ltd.,Xi'an, China. E-mail: 872704996@qq.com
c, Key Laboratory on Resources Chemicals and Materials of Ministry of Education, Shenyang University of Chemical Technology, Shenyang, 110142, China.
d, Laboratory of Engineering Thermochemistry, Guangdong University of Technology, Guangzhou, 510006, People's Republic of China.

1. Experimental Section

1.1 Materials

$Ba(OH)_2$, $Ni(NO)_3 \cdot 6H_2O$, urea,and nickel foam(NF) (99.9 wt%, 1.0 mm in thickness). All the reagents were used as received without further purification. Deionized (DI) water was used for the preparation of all aqueous solutions. All the reagents used in the experiment were commercial chemicals without further purification. Deionized water was used throughout the experimental processes.

2. Characterization

X-ray diffraction patterns (XRD) were obtained on a Rigaku corporation SmartLab and diffractometer with Cu Kα radiation (λ = 0.154 nm). The morphology of the as-prepared catalysts was obtained by scanning electron microscopy (SEM, JEOL, SU-8000, and S4800) operating with 5 kV and 2 kV at 25 oC (room temperature). Energy dispersive X-ray spectroscopy spectrum and mapping (EDX spectrum, EDX-mapping) images

were obtained using the Horiba. Transmission electron microscopy (TEM) and corresponding energy-dispersive X-ray spectroscopy (EDS) elemental mapping were performed on FEI Tecnai G20 electron microscope operating with 200 kV at room temperature. X-ray photoelectron spectroscopy (XPS) analysis was executed using an ESCALAB Xi+ instrument with a monochromatic Al-Ka X-ray excitation. Upon obtaining XPS data, we initially read the peak coordinates of C1s, compared this value with the standard value of 284.8eV, and performed differential correction. Subsequently, we applied this difference to correct all the data. After the correction, we used XPSpeak software for fitting. The process involved importing the data, establishing a baseline, selecting "Shirley type" in the Background type under the software's menu bar, and adjusting the baseline by modifying the slope value. Following this, peak fitting was performed according to references[1-7]. The fitted data was then matched to align with the peaks, obeying XPS deconvolution rules. Finally, the data was saved, exported, and plotted in Origin to obtain the XPS spectrum.

3.Electrochemical measurements

The electrochemical test was carried out at room temperature with a typical three electrode system, which used the NF supported catalyst as the working electrode(1 cm*0.5 cm), a platinum gauze electrode as the counter electrode(10 mm*10 mm, 0.1 mm) and a Mercury/Mercury Oxide (Hg/HgO) as reference electrode. All of the electrochemical testings were carried out on the CHI 660E electrochemical workstation (Shanghai CH Instrument, China). All polarization curves have been corrected by iR compensation at room temperature, and the potential has been transformed into the potential relative to the standard hydrogen reference electrode according to the Nernst equation. The conversion formula is described as follow: E RHE = E Hg/HgO + 0.098 + 0.059*pH. For the UOR tests, the LSV curves were measured between 1.0 and 1.8 (vs. RHE) at a scan rate of 5 mV s-1 in 1.0 M KOH solution with 0.33M urea. The Tafel plot was accorded with the equation $\eta = b \log j + a$, where η was the overpotential, b was the Tafel slope, and j was the current density. The double-layer capacitance (Cdl)

was determined by cyclic voltammetry in the voltage range between 1.02 and 1.12 (vs. RHE) in 1.0 M KOH mixed solution, and the current density variation (ΔJ = Ja – Jc) at an overpotential (intermediate value of the applied potential range) were plotted against scan rate, then the slope of the line was divided by 2 to get the Cdl value.

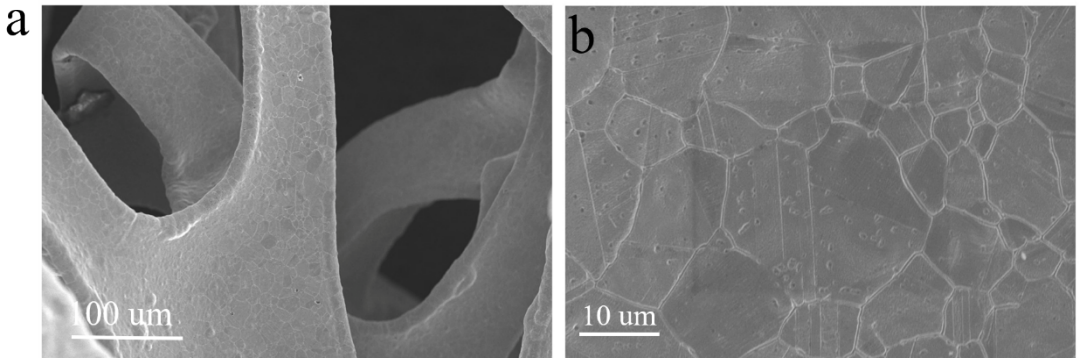

Figure S1. Morphology and structure characterizations. SEM images of (a, b) NF at different magnifications.

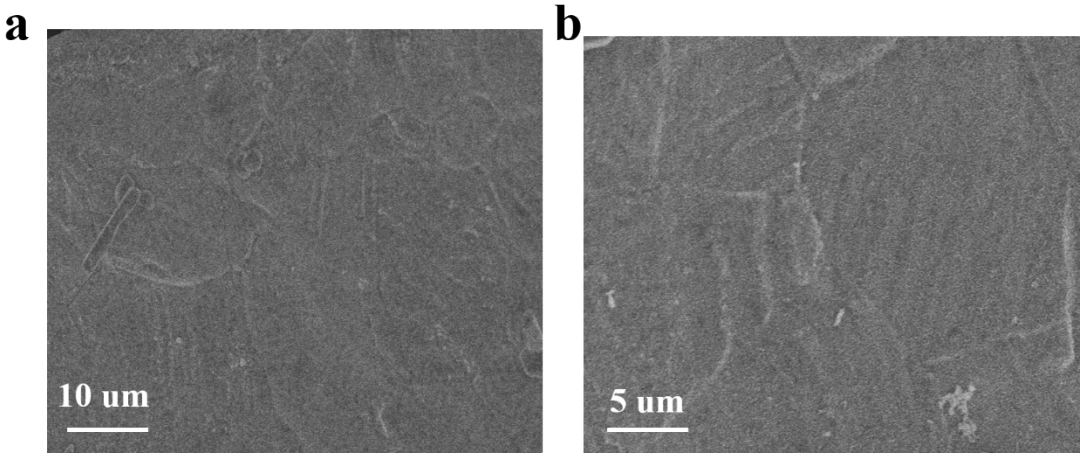

Figure S2. Morphology and structure characterizations. SEM images of (a, b)Ba/NF at different magnifications.

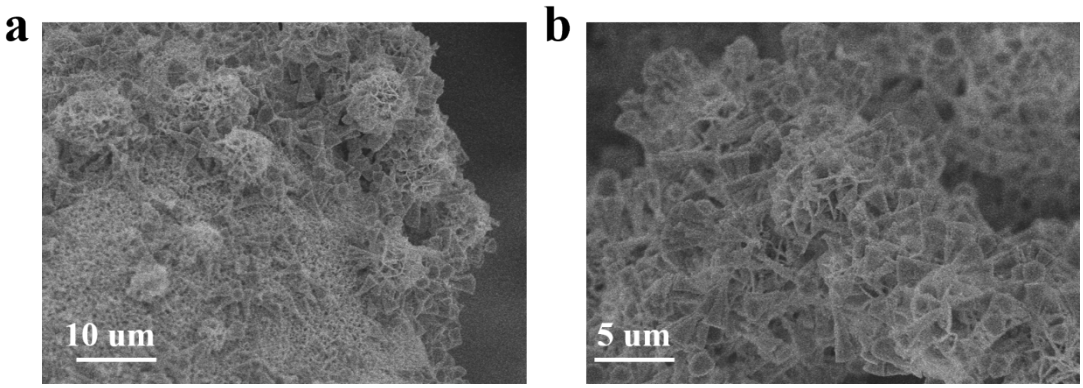

Figure S3. Morphology and structure characterizations. SEM images of (a, b)Ni/NF at different

magnifications.

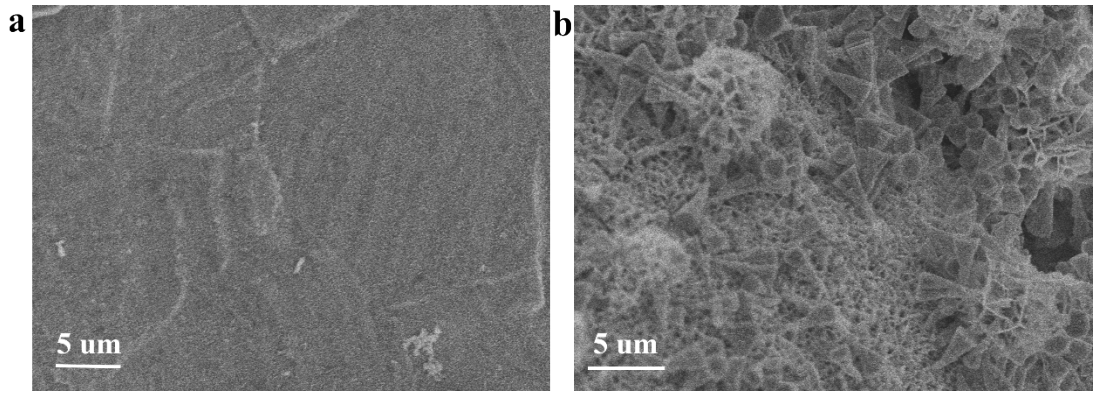

Figure S4. Morphology and structure characterizations. SEM images of (a)Ba/NF and (b) Ni/NF

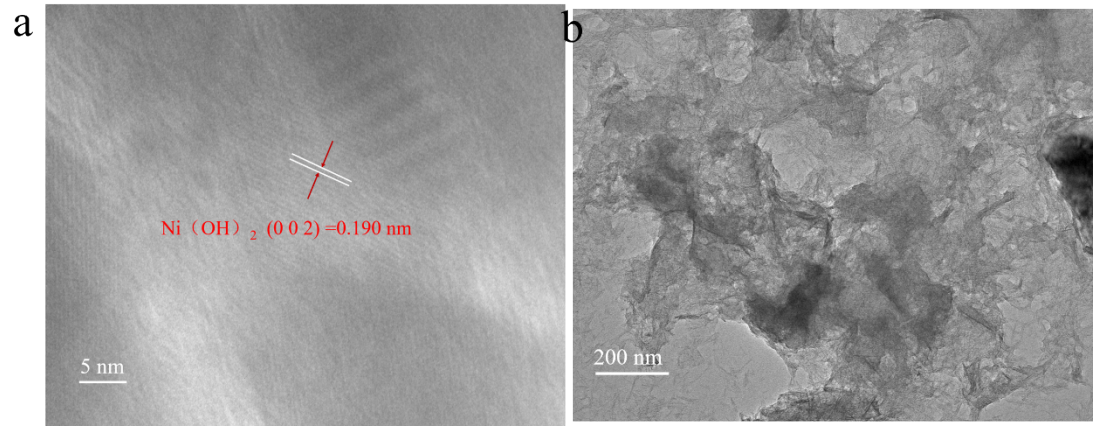

Figure S5.(a) Typical HRTEM images taken from the Ni/NF catalyst.(b) TEM image of an ultrasonication-exfoliated nanoflake of Ni/NF.

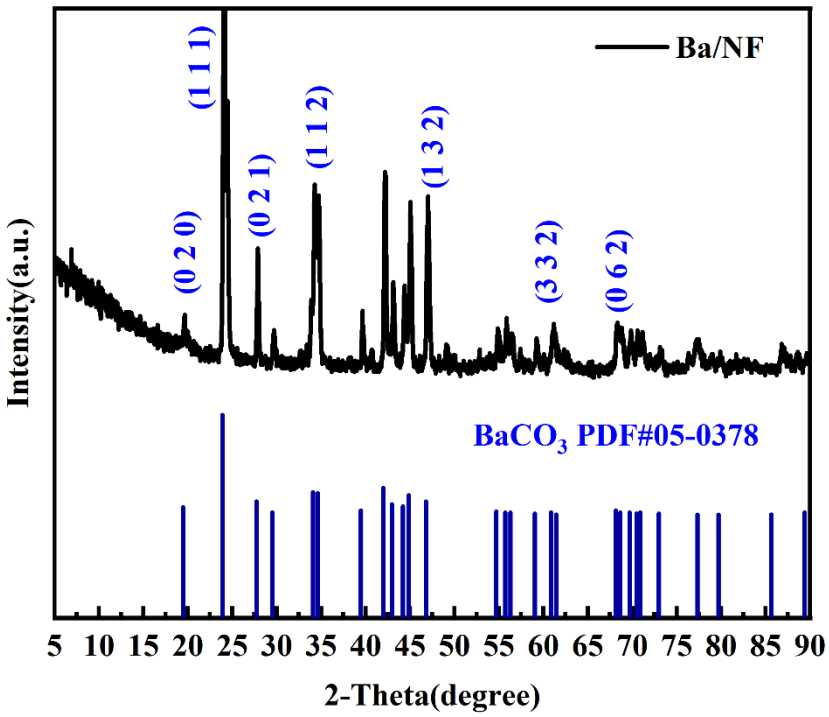

Figure S6. XRD of Ba/NF.

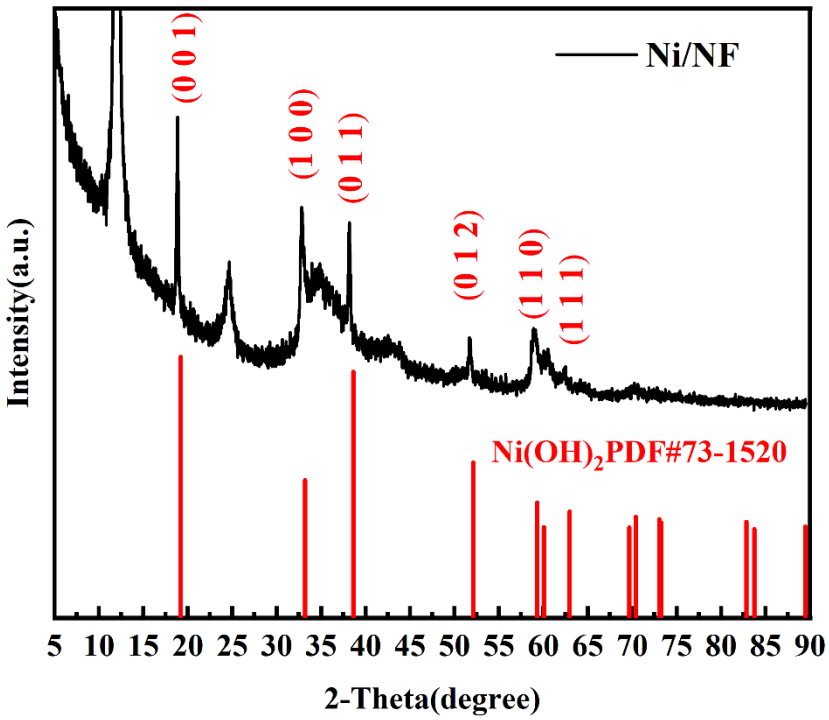

Figure S7. XRD of Ni/NF.

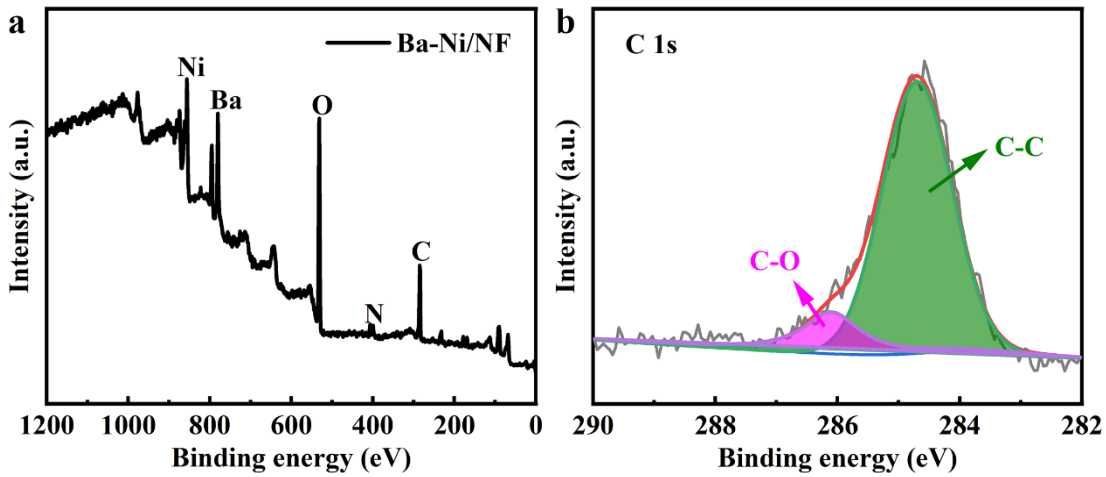

Figure S8. (a) XPS survey spectrum of Ba-Ni/NF and XPS spectra of Ba-Ni/NF for (b) C 1s regions.

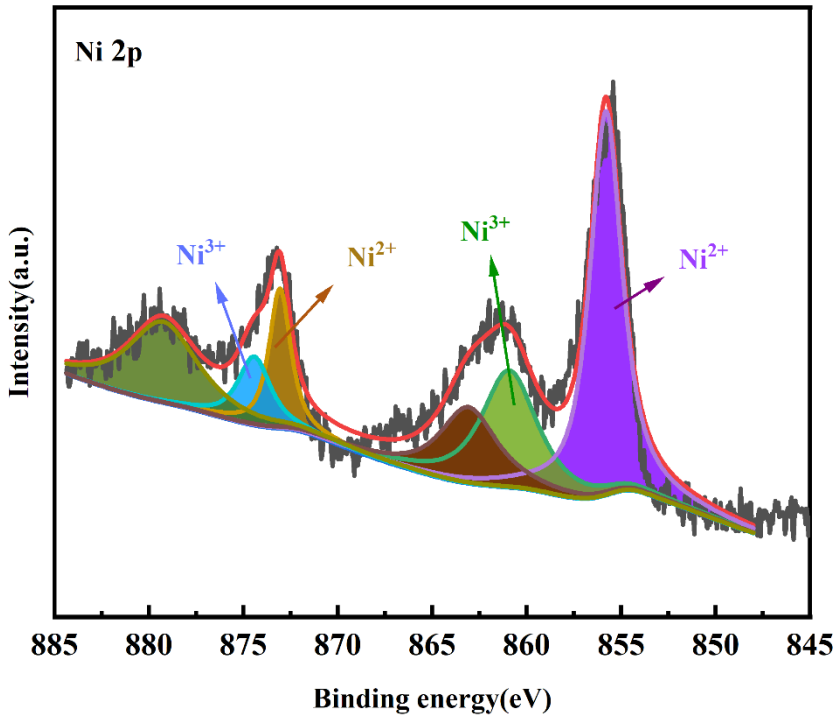

Figure S9. XPS spectra of Ni/NF for Ni 2p

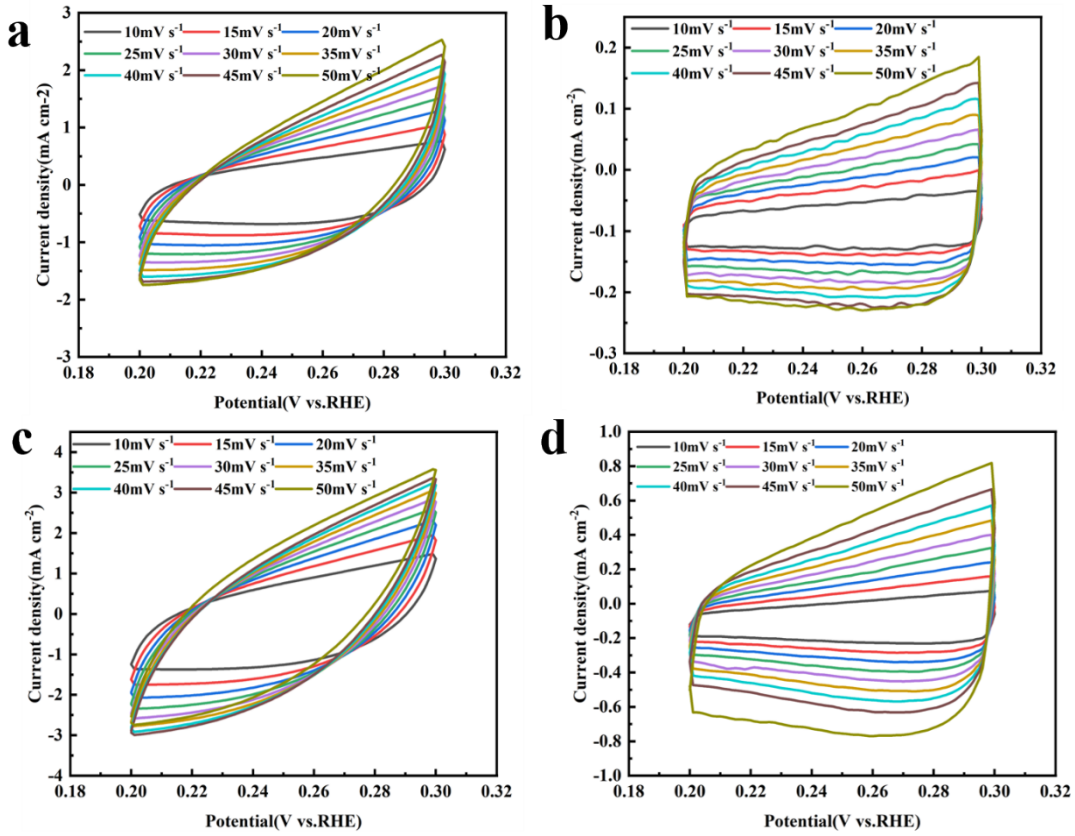

Figure S10. CV curves of (a) Ba-Ni/NF(Ni:Ba=2.5:1), (b) Ba/NF, (c) Ni/NF, (d) NFat different scan rates.

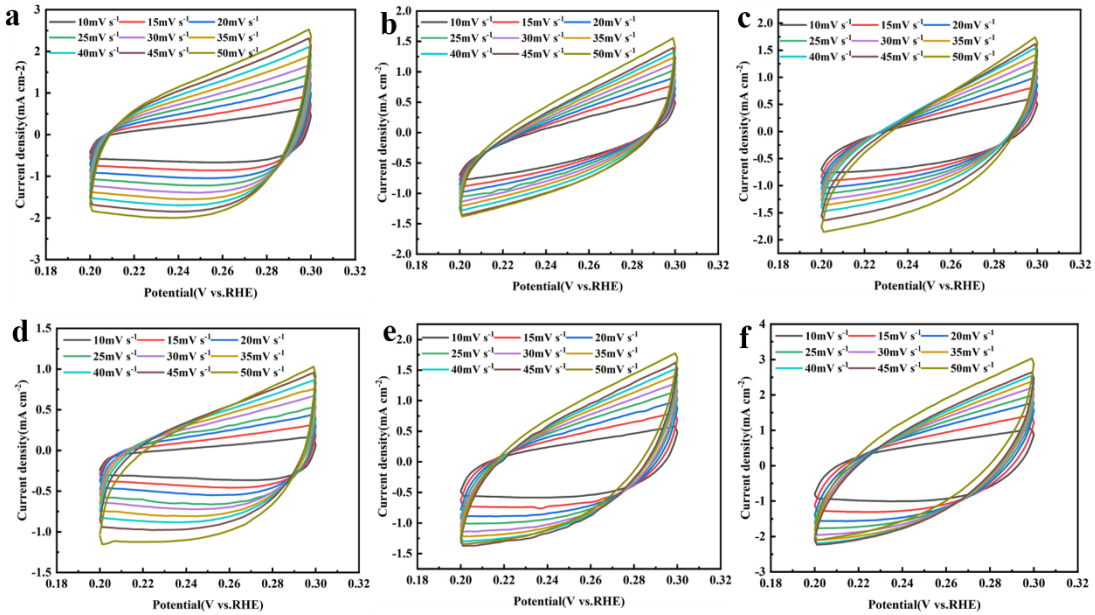

Figure S11. The cyclic voltammetry (CV) plots of Ba-Ni/NF with different Ni-Ba concentration ratios are as follows: (a) 1:1, (b) 1:2, (c) 1:2.5, (d) 1:3, (e) 2:1, and (f) 3:1.

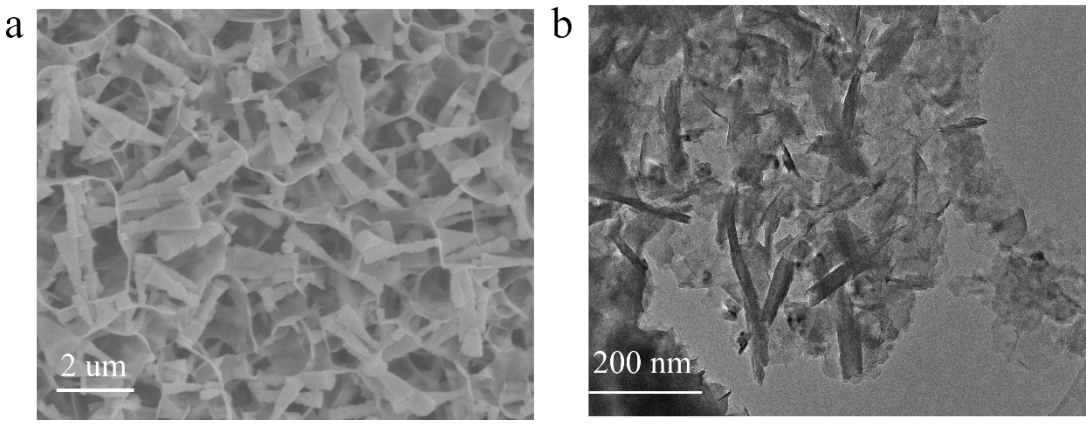

Figure S12. (a) SEM image and (b) TEM image of Ba-Ni/NF after stability testing.

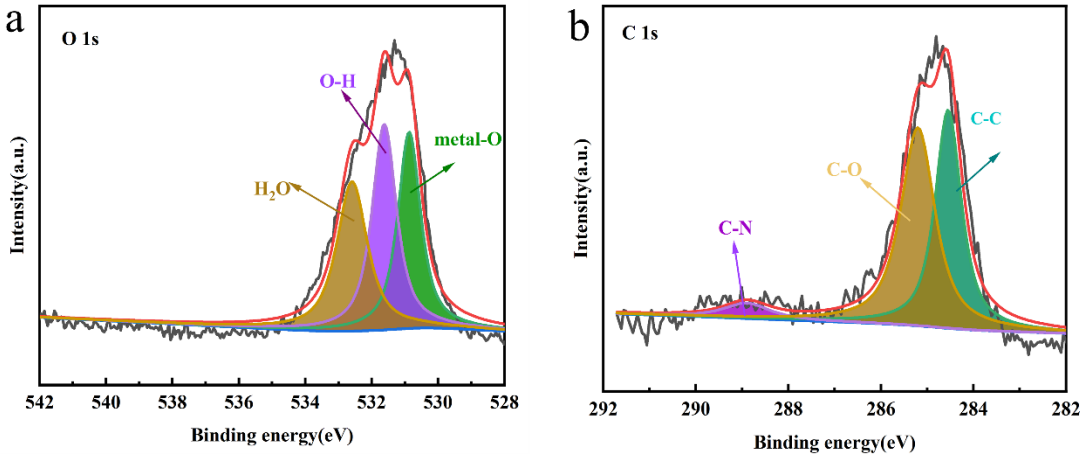

Figure S13. XPS spectra of Ba-Ni/NF after stability testing for (a) O 1s, (b) C 1s.

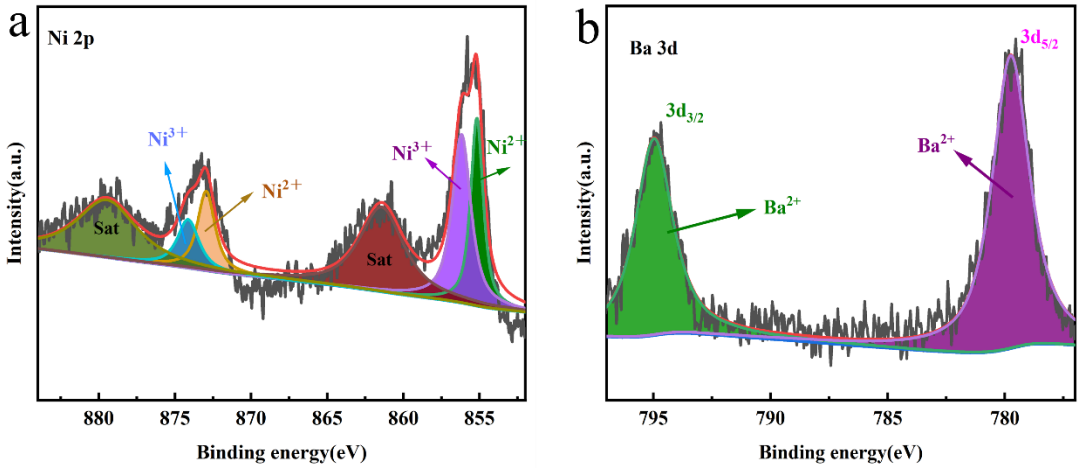

Figure S14. XPS spectra of Ba-Ni/NF after stability testing for (a) Ni 2p, (b) Ba 3d.

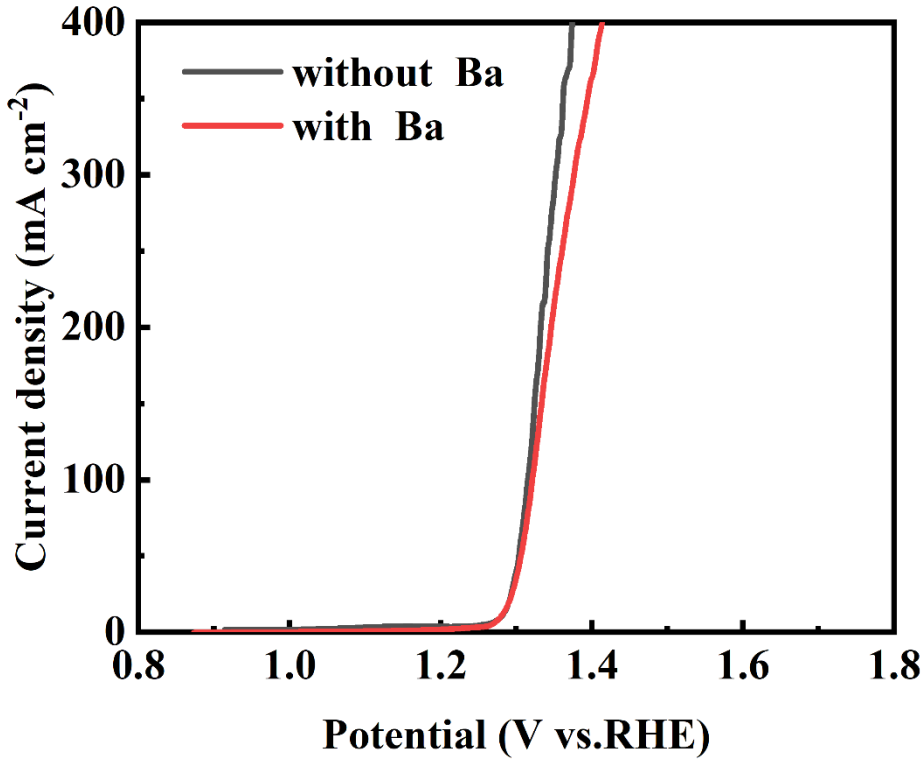

Figure S15. LSV of Ba-Ni/NF in electrolytes with and without Ba.

Table S1. The ratios of various elements in the Ba-Ni/NF sample measured by XPS.

Name	C 1s	N 1s	O 1s	Ni 2p	Ba 3d
Atomic%	7.57	2.92	24.5	44.28	20.73

Table S2. The ratio of various elements in the Ba-Ni/NF sample after stability test measured by XPS.

Name	C 1s	N 1s	O 1s	Ni 2p	Ba 3d
Atomic%	11.82	2.8	25.15	44.34	15.89

Table S3. The ratio of Ba elements in the Ba-Ni/NF sample after test measured in electrolytes with Ba.

Name	Ba
Atomic%	16.21

Table S4. The solution resistance of Ba-Ni/NF in alkaline solutions with and without urea.

With urea	Without urea
2.218 Ω	2.098 Ω

4. DFT calculations

To investigate the UOR reaction mechanism on $Ni(OH)_2$ site and $Ba/Ni(OH)_2$ site, a $Ba/Ni(OH)_2$ model was built, which contains six Ni(II) and two Ba (II). And the reaction is assumed to be taken placed on the Ba(II) center. All DFT calculations were carried at PBE0/def2-SVP level with Grimme's D3BJ1 empirical dispersion correction using the Gaussian 16 program2. Gibbs free energy is evaluated by frequency calculations. The Gibbs free reaction energy for each elementary electrode step was calculated using the computational hydrogen electrode model: $\Delta G = GP^* - GR^* + 1/2G_{H2} - kT^*pH + eU$.

where GR* is the Gibbs free energy of absorbed reactant. GP* is the Gibbs free energy of absorbed product. G_{H2} is the Gibbs free energy of H_2 molecule. e is transferred electron and U is the applied overpotential, where U = 0 V, that is, zero overpotential referenced with the reversible hydrogen electrode and non-charged models are applied.

Table S5. Comparison of UOR performance of Ba-Ni/NF with recently reported catalysts.

Catalyst	**Urea Concentration (mol/L)**	**E@J (V vs.RHE @mA/cm^2)**	**Ref.**
Ba-Ni/NF	**0.33**	**1.316@100**	**This work**
Ni(OH)s/NF	0.33	1.34@10	[8]
NiOOH/(LDH/α-FeOOH)	0.33	1.40@100	[9]
β-NiMnOOH	0.33	1.34@100	[10]

NiMoCu/NF	0.33	1.40@100	[11]
V-$Ni(OH)_2$	0.33	1.43@100	[12]
FeMn-PS	0.33	1.35@100	[13]
Fe-$NiCo_2S_4/Ni_3S_2$	0.33	1.39@100	[14]
NiCo	0.33	1.373@10	[15]
Ni_2P	0.5	1.6@95.47	[16]
NiS/MoS_2	0.4	1.43@100	[17]
Fe-Co/LDH	0.33	1.353@50	[18]
Ni-bza	0.33	1.38@10	[19]
VOOH-Ni	0.33	1.356@10	[20]
Co_3O_4-CT1	0.5	1.34@100	[21]
MoO_3/Ni-N-C	0.5	1.42@50	[22]

References

1. Á. A. Amaya, C. A. González, M. E. Niño-Gómez and F. Martínez O., J. Electron. Spectrosc., 2019, **233**, 5–10.
2. X. Gu, Z. Liu, M. Li, J. Tian and L. Feng, Appl. Catal. B-Environmental, 2021, **297**, 120462.
3. J. Jiang, Y.-J. Zhang, X.-J. Zhu, S. Lu, L.-L. Long and J.-J. Chen, Nano Energy, 2021, **81**, 105619.
4. C. V. Ramana, M. Bandi, A. N Nair, F. S. Manciu, S. Sreenivasan and V. Shutthanandan, ACS Appl. Energy Mater., 2021, **4**, 1313–1322.
5. Y. Chen, J. Fang, S. Lu, C. Cen, C. Cheng, L. Ren, W. Feng and Z. Fang, RSC Adv., 2016, **6**, 15745–15752.
6. J. Ma, L. Wang, F. Yu and X. Dai, Chem. Eng. J., 2019, **370**, 938–943.
7. S. Chenakin and N. Kruse, J. Phys. Chem. C, 2019, **123**, 30926–30936.
8. X. Jia, H. Kang, X. Yang, Y. Li, K. Cui, X. Wu, W. Qin and G. Wu, *Appl. Catal. B-Environmental*, 2022, **312**, 121389.

9. M. Cai, Q. Zhu, X. Wang, Z. Shao, L. Yao, H. Zeng, X. Wu, J. Chen, K. Huang and S. Feng, *Adv. Mater.*, 2023, **35**, 2209338.

10. X. Yan, L. Xiang, W.-D. Zhang, H. Xu, Y. Yao, J. Liu and Z.-G. Gu, *J. Colloid Interf. Sci.*, 2023, **629**, 370–378.

11. R. Li, Y. Yuan, H. Gui, Y. Liu, H. Li, Y. Li, S. Wen, A. Liu, J. Zhang, P. Yang and M. An, *Nanoscale*, 2022, **14**, 14297–14304.

12. Q. Cao, Y. Yuan, K. Wang, W. Huang, Y. Zhao, X. Sun, R. Ding, W. Lin, E. Liu and P. Gao, *J. Colloid Interf. Sci.*, 2022, **618**, 411–418.

13. X. Meng, M. Wang, Y. Zhang, Z. Li, X. Ding, W. Zhang, C. Li and Z. Li, *Dalton Trans.*, 2022, **51**, 16605–16611.

14. Y. Wang, N. Chen, X. Du, X. Han and X. Zhang, *J. Alloys Compd.*, 2022, **893**, 162269.

15. Q. T. Luong, H. J. Choi, T. B. N. Huynh, J. Song, Y.-H. Cho and O. J. Kwon, *Electrochimica Acta*, 2022, **431**, 141159.

16. H. Liu, S. Zhu, Z. Cui, Z. Li, S. Wu and Y. Liang, *Nanoscale*, 2021, **13**, 1759–1769.

17. Y. Zheng, P. Tang, X. Xu and X. Sang, *J. Solid State Chem.*, 2020, **292**, 121644.

18. Y. Gong, H. Zhao, D. Ye, H. Duan, Y. Tang, T. He, L. A. Shah and J. Zhang, *Appl. Catal. A-Gen.*, 2022, **643**, 118745.

19. J.-L. Liu, X.-Y. Zhou, J.-L. An, Y.-Q. Wang, M.-D. Zhang and L. Qin, *Energy Fuels*, 2022, **36**, 10346–10353.

20. D. Wei, W. Tang, N. Ma and Y. Wang, *Mater. Lett.*, 2021, **291**, 129593.

21. M. Fang, W.-B. Xu, S. Han, P. Cao, W. Xu, D. Zhu, Y. Lu and W. Liu, *Mater. Chem. Front.*, 2021, **5**, 3717–3724.

22. Y. Bao, K. Chen, Z. Feng, H. Ru, M. Guo, D. Chen, X. Li, J. Tu, L. Ding and X. Lai, *ACS Appl. Nano Mater.*, 2023, **6**, 11221–11229.